

Accuracy of the Shack-Hartmann Wavefront Sensor^a

6.1

INTRODUCTION

The wavefront aberration function is a fundamental description of the eye's optical characteristics from which traditional measures of image quality, such as the point spread function or the optical transfer function, may be calculated (Williams & Becklund, 1989; Goodman, 1996). However, the inverse problem of determining the wave aberration, given the point spread or optical transfer function, does not yield a unique solution, and for this reason the wave aberration function is a richer description of the optical properties of the eye. Furthermore, for applications such as supernormal vision and high-resolution imaging of the fundus (Liang, Williams, & Miller, 1997), which require aberration correction, methods for direct measurement of the wavefront aberration of the human eye are required. Currently available methods fall into two broad categories, subjective and objective, but they are all based on a common principle: The direction of rays passing through select points in the pupil are monitored, and aberrations are quantified by the deviation of these select rays from the trace of rays in an aberration-free system.

Subjective methods for measuring ray aberrations all require that the subject judge the apparent visual direction of discrete points in the retinal image that result from rays passing through specific points in the pupil plane. In the aberroscope method, for example, a grid is placed over the pupil and the eye is deliberately defocused in order to produce a blur circle that replicates the shape of the pupil, including the grid of opaque lines (Tscherning, 1894; Howland & Howland, 1977). Since each intersection of grid lines corresponds to a specific pupil location, distortions seen in the retinal shadows of the grid may be used to infer the directions of identified rays as they leave the eye's pupil and eventually intersect the retina. In

^a With only minor changes, this chapter was published under the title, "Comparison of the eye's wave-front aberration measured psychophysically and with the Shack-Hartmann wave-front sensor" (Salmon, Thibos & Bradley 1998).

effect, the subjective aberroscope is an entoptic ray-tracing device that allows the simultaneous monitoring of multiple rays as they pass through known pupil locations. The subject's task in this case is to estimate the apparent visual direction of each point on the grid by perceptually interpreting the retinal stimulus as if it were the conventional image of a real object formed by the eye's optical system. An alternative approach developed originally by Smirnov (Smirnov, 1961; Webb, Penney, & Thompson, 1992; Woods, Bradley, & Atchison, 1996) uses a modified Scheiner principle to implement a nulling technique which avoids the requirement for magnitude estimation of visual direction. In this method a single pinhole aperture is used to isolate a narrow bundle of rays from an axial point source as they pass through a known location in the eye's pupil. In an aberrated eye, the retinal intersection of this ray bundle will not coincide with the paraxial retinal image of a reference point source. The subject will therefore perceive the test and reference point sources as having different visual directions. To nullify this difference in visual direction, the subject displaces the test light until it appears to coincide with the reference light. In this way the ray aberration is transferred from image space to object space, where it may be measured quantitatively (Thibos, Bradley, Still, Zhang, & Howarth, 1990). Unfortunately, the method of subjective magnitude estimation (used in the aberroscope) is inherently unreliable, and the nulling method (used in the Smirnov technique) is very time consuming^b (Charman, 1991). Consequently, both methods place an excessive demand on the subject, which makes both techniques unsuitable for routine use with patients in a clinical setting.

In response to the manifest problems of subjective techniques, two objective methods for measuring the wavefront aberration function of the eye have been developed. The first is an objective aberroscope that uses a fundus camera to record an image of the distorted grid on the retina (Walsh, Charman, & Howland, 1984; Atchison, Collins, Wildsoet, Christensen, & Waterworth, 1995; Walsh & Cox, 1995). One of the limitations of the objective aberroscope is that the eye's optical system serves as the objective lens for the fundus camera. Consequently, the eye's imaging quality limits the minimum usable spacing between grid lines in the pupil plane to about 1 mm, thus limiting the resolution with which the eye's aberrations may be specified (Charman, 1991). For the same reason, a highly aberrated eye may not yield an image of sufficient quality to allow reliable measurements of the aberration function. Both of these problems with the aberroscope method are avoided by the second objective method, the Shack-Hartmann (S-H) wavefront sensor, which characterizes the eye's aberrations in object space. Developed originally for astronomical applications and adapted recently for the eye by Liang *et al.*, (1991), this wavefront sensor uses an array of lenses and a video detector to measure rays of reflected light emerging

^b Recently a redesigned, partially automated version of the Webb spatially resolved refractometer was used to subjectively measure the wavefront aberration at 39 pupillary locations, on a two dimension grid, in about 4 minutes (He, *et al.*, 1998)

from the eye. In the S-H method a narrow beam of light is directed into the eye to produce a high-quality point source of light on the fundus. Light reflected from the fundus is then subdivided into a large number of ray bundles as it leaves the eye. This is achieved by placing an array of tiny lenses in a plane conjugate with the eye's pupil plane. A video detector (CCD) located at the focal plane of the lenslet array thus records an array of point images, one for each lens in the array. For an eye free of defocus and aberrations, all of the exiting ray bundles would be parallel, and therefore the CCD would record an array of point images with the same geometry as the lenslet array. Deviations from this geometry may therefore be attributed to aberrations in the exiting beam. Given that high-density lenslet arrays are available commercially, the S-H method for measuring the wave aberration function in human eyes is emerging as the method of choice, since it is fast, objective, and has high spatial resolution in the pupil plane.

Measurement of the eye's wavefront aberration function is becoming an important goal of clinical optometry and ophthalmology (Thibos, 1997) and is a critical first step towards the optical correction of ocular aberrations using adaptive or active optics (Liang, *et al.*, 1997; Wu, 1997). Given the great potential of wavefront sensing for advancing fundamental and applied research in visual optics, it becomes essential that the validity of this new technique be thoroughly assessed with human eyes. Recently Liang and Williams tested repeatability of the S-H technique by repeated measurements of the wavefront aberration function along the eye's vertical meridian (Liang & Williams, 1997). They reported average standard deviations of $\sim\lambda/14$ ($n=20$, 3.4 mm pupil) and $\sim\lambda/12$ ($n=3$, 7.3 mm pupil) for two observers. They also tested accuracy by two methods. First, they measured the wavefront of a laser beam which had been defocused by known amounts across an 8 diopter (D) range. Error was less than 0.17 D. Next, they compared modulation transfer functions (MTF's) for human eyes derived from S-H measurements with MTF's derived from double pass and interferometer measurements recorded previously on the same three observers (Williams, Brainard, McMahon, & Navarro, 1994). Comparisons were limited to a single vertical cross section of the MTF's. They found reasonable, though not perfect agreement and discussed theoretical considerations which could account for the discrepancies. Although all of these tests provided valuable evidence of the S-H sensor's validity, none directly assessed the ability of the wavefront sensor to accurately measure the wavefront aberration of the human eye. Indeed, there is reason to be skeptical, given the complexity of the fundus as a multiple-layered reflector with scattering, specular, and wave-guide attributes (van Blokland & van Norren, 1986; Gorrand & Delori, 1995), and the fact that object-space and image-space characterizations of the eye's aberrations rely on different ray paths and therefore might reasonably be expected to differ.

My purpose was to evaluate accuracy of the S-H method by directly comparing the wave aberration function measured objectively with that measured by an alternative method. I chose the Smirnov technique for this purpose because, although it is time consuming, the nulling psychophysical method produces

reliable results with negligible measurement variance (e.g. a typical vernier threshold of 15 arc seconds in these experiments corresponds to an mean wavefront aberration measurement error of less than $\lambda/20$). The experiment consisted of three parts. First, prior to measuring human eyes, accuracy of the S-H system was tested by measuring wavefronts which had known spherical curvatures. Next, multiple S-H images for two observers were collected, and mean wavefronts and standard errors were computed to assess repeatability with human eyes. Finally, wave aberration functions for the same subjects were measured psychophysically, and the results compared to the S-H aberration functions to evaluate accuracy with human eyes.

6.2

METHODS

6.2.1 Comparison of the two methods

In principle, the Smirnov and S-H methods are optically equivalent except for the direction of ray propagation: the S-H technique measures the deviation of rays exiting the eye, and the Smirnov technique measures the deviation of rays entering the eye. In both cases the geometry of ray deviations is the same, as illustrated schematically in Fig. 6.1, and the ray aberrations as specified in object space are the same. To see why this is true, consider first the subjective Smirnov method (Fig. 6.1, bottom) in which a distant axial point source serves as a fixed reference point. In an aberration-free eye, the dashed rays from the reference source travel parallel to the axis in object space and converge on the fovea in image space. To achieve the same end in an aberrated system, rays must enter the entrance pupil of the eye obliquely. For example, if a particular point in the entrance pupil is isolated by a pinhole aperture, rays from a test target must enter at an angle $\theta = \Delta s/d$ to the reference ray to intersect the retina at the fovea. Now consider the S-H method (Fig. 6.1, top) in which rays of light emanate from the fovea and exit the eye through the same point in the entrance pupil. (For the purposes of explaining the Shack-Hartmann principle, Fig. 6.1 shows the lenslet array inside the eye, but it is actually located outside the eye in a plane conjugate with the entrance pupil.) The emerging bundle of rays is focused by a lenslet in the array onto the CCD sensor, and for an aberration-free eye the image would fall upon point y_0 . In the case of an aberrated eye, however, the image is displaced from the reference location by an amount Δy and the ray deviation angle $\theta = \Delta y/f$. Thus, although there are differences of implementation, both methods measure the same angle θ , which represents the ray aberration at the given pupil location. Given that rays are orthogonal to wavefronts, θ also represents the slope of the wavefront W in object space, from which W may be derived by integration. Since the reference wavefront in object space is planar, W also represents the axial distance between the aberrated wavefront and the reference wavefront and therefore, by definition, is equal to the wavefront aberration function.

6.2.2 The Shack-Hartmann wavefront sensor

The layout of my Shack-Hartmann (S-H) wavefront sensor is shown in Fig. 6.2 and photographs of the apparatus are in Appendix G. The apparatus may be divided into two main parts: an illumination branch, which projected a point of light onto the retina; and a sensor branch, which measured the eye's wavefront aberration. The illumination branch included the components between the laser and eye. The beam from a helium-neon laser (632.8 nm, 10 mW) passed through neutral density filters, an electronically controlled shutter and a spatial filter that consisted of a microscope objective (focal length, 8 mm) and a 25- μm pinhole. Lenses L1-L3 (achromatic doublets; focal length, 100 mm) along with an ophthalmic lens (Rx) and the eye's optics, formed an image of the pinhole on the subject's retina. Aperture A1 limited the beam diameter to 2 mm to ensure that the point source imaged on the retina would be a diffraction-limited spot (i.e. Airy's disk). Lens L2 allowed the subject to fine tune the focus of the incoming beam subjectively. Beyond lens L3, a pellicle beam splitter (8% reflectance, 92% transmittance) reflected the beam into the eye. A laser power meter verified that power entering the eye was less than 6 μW , which for a 2.0-second exposure is 1% of the American National Standards Institute maximum permissible exposure (Sliney & Wolbarsht, 1981; ANSI, 1993). A summary of laser safety calculations is included as Appendix H.

The sensor branch included optics between the eye and the slow-scan CCD camera (Model MCD600, SpectraSource Instruments). The CCD sensor (Kodak KAF 1400) was composed of 6.8- μm square pixels arranged in a 1340 \times 1037 array. Lenses L4 and L5 were achromatic doublets (focal lengths, 100 mm). Lens L4 was one focal length from the eye's entrance pupil. Lenses L4 and L5 were separated by two focal lengths, and the lenslet array was one focal length from L5. The CCD was placed in the focal plane of the lenslets. The lenslet array (MLM 0400-24-S-1, Adaptive Optics Associates) contained 0.4-mm square lenslets with focal lengths of 24 mm. With this arrangement the CCD was conjugate to the retina, while a unit-magnification image of the pupil was formed in the plane of the lenslets. A 1-mm confocal aperture (A2) blocked the corneal Purkinje image but transmitted light from the retina. Lens Rx was used to correct the subject's spherical refractive error for both the ingoing and outgoing beams.

At the beginning of an experimental session a reference image was captured by introducing a plane wave into lens L4 of the sensor branch. The image of the lenslet focal spots was analyzed using a Macintosh computer to locate the x and y positions of each dot centroid. This provided the reference positions from which dot displacements would be measured.

The subject's head was stabilized with a bite bar, and the right eye was positioned so that the primary line of sight (also known as the fixation axis) coincided with the sensor's optic axis. The line of sight is defined in object space as the line connecting the fixated object point with the entrance pupil center.

The line of sight is the preferred reference axis for specifying the eye's wave aberration function (Mandell, 1992; Mandell, 1994; Applegate *et al.*, 2000—in press) because the aberration function is traditionally specified with respect to the center of the pupil, and the line of sight, by definition, connects the fixation point to the center of the eye's entrance pupil and connects the center of the exit pupil to the fovea. Line-of-sight alignment was accomplished as follows. Laser radiance was attenuated to a safe level for continuous viewing, and the shutter was opened while the subject fixated the pinhole. The subject attended to the position of aperture A2, which was translated axially back and forth between lenses L4 and L5. The eye's horizontal (x) and vertical (y) positions were adjusted until, for all locations of aperture A2, its blurred image always appeared to be centered on the red pinhole. Since the experiment would be conducted in total darkness except for the brief image exposure, it was necessary to provide the subject with another fixation target, which was optically aligned with the line of sight. It consisted of a dimly illuminated cross that was reflected into the illumination branch by a pellicle placed between lenses L2 and L3. Since I did not paralyze accommodation, the fixation target was slightly defocused in the myopic direction to minimize any stimulus to accommodation.

The eye's entrance pupil was placed at the focal plane of lens L4 by the following procedure. Aperture A2 was temporarily replaced with a mirror so that the experimenter could view the eye through a telescope (focused at optical infinity), lens L4, and the ophthalmic trial lens Rx. The eye was translated along the optic axis until the iris margin was seen clearly focused by the experimenter.

The electronic shutter and camera shutter were synchronized for 1-2-second exposures, and five images for each subject were taken. Following each exposure the subject would dismount from the bite bar and rest 2-4 minutes while the experimenter evaluated and preprocessed the images. Example raw images are shown in Figs. 6.4a, and 6.4d.

A computer program (MATLAB, Mathworks, Inc.) was written to locate the dot centroids with minimal user input, and wavefront aberration functions were computed by the following steps:

- 1) Horizontal (x) and vertical (y) displacements for each dot from the reference positions were computed;
- 2) Displacements, divided by lenslet focal length (24 mm), converted the data into deviation angles in the x and y directions, which were interpreted as wavefront slopes or partial derivatives of the wavefront with respect to x and y.
- 3) The wavefront aberration function was determined by numerical integration of the partial derivatives across the pupil to produce a two-dimensional array of wavefront aberration values in micrometers. With normalization by one wavelength (0.6328 μm) these values were converted to wavelengths.

6.2.3 Psychophysical apparatus and procedures

Figure 6.3 shows a schematic of the psychophysical apparatus, which is similar to that used by Woods *et al.* (1996). The subject directly viewed a fixed white annular target that had an inner diameter of 3.5 minutes of arc (arc min). The annulus was seen through the entire pupil, and the subject was instructed to fixate the center of the target. Through a second optical channel the subject also saw a red light-emitting diode (LED; dominant wavelength, 640 nm) that had a diameter of approximately 3 arc min. Light from the LED was polarized and blocked from entering most of the pupil by a crossed polarizer positioned before the eye. A 0.6-mm pinhole in this polarizing filter allowed light from the LED to enter the pupil in only one discrete location. To locate the center of the eye's entrance pupil the pinhole aperture was displaced right and left until the pinhole was vignetted by the iris. This process was repeated for a vertical traverse, and the midpoint of the two traverses was taken as the pupil center. The line connecting this pupil center to the annulus center thus defined the fixed line of sight for the experiment. To conduct the experiment, the experimenter then positioned the pinhole aperture at a predetermined sequence of positions along the horizontal meridian of the eye's pupil. At each position the LED appeared to the subject to be displaced from the annulus center by an amount that was indicative of the degree of aberration at that pupil location. The subject repositioned the LED until it appeared to be centered in the annulus, and the LED's new x and y coordinates were recorded. This process was repeated for approximately 15 locations of the pinhole across the horizontal midline of a 5.6-mm pupil. Since this procedure required approximately 3 hours, I limited psychophysical measurements to the horizontal meridian of the pupil.

Measured deviation angles θ in the horizontal direction were interpreted as local wavefront slopes that could be fitted by the method of least squares to a fifth order polynomial of the form

$$\theta = dW/du = B_0 + B_1u + B_2u^2 + B_3u^3 + B_4u^4 + B_5u^5 \quad (6.1)$$

where dW/du represents the wavefront slope in radians; u is the horizontal pupil location measured in micrometers; and the B coefficients are associated with the classic aberrations: prism (B_0), defocus (B_1), primary coma (B_2), primary spherical aberration (B_3), secondary coma (B_4) and secondary spherical aberration (B_5). With omission of the prism and defocus terms and with normalization by one wavelength, the resulting polynomial was integrated to give a one-dimensional wavefront aberration function $W(u)$ in wavelengths of the form,

$$W(u) = B_2u^3/3 + B_3u^4/4 + B_4u^5/5 + B_5u^6/6. \quad (6.2)$$

To permit direct comparison of the aberrations measured by the two methods, the two-dimensional S-H wavefront slope data were interpolated along the horizontal meridian to produce one-dimensional data that were also fitted with Eq. (6-1) and integrated to the form of Eq. (6-2).

6.2.4 Experimental protocol

Experiments were performed on the right eye of two subjects without cycloplegia. Under dark-room illumination the diameter of the natural pupil was about 5.6 mm. This permitted sampling of approximately 150 pupil locations with the S-H method, which is more than sufficient to represent the significant ocular aberrations (up to the tenth order) reported by Liang and Williams (Liang & Williams, 1997). Each of the five S-H images were processed to yield a wavefront aberration function. The five aberration functions were interpolated using bicubic interpolation to 0.2-mm spacings, and the mean and standard errors ($n = 5$) were computed. Data for the Smirnov experiment were collected in a single 3-hour session for subject DH and in two 3-hour sessions on the same day for LT. Information about the subjects is summarized in Table 6.1.

TABLE 6.1 Summary data for two subjects whose right eyes were measured with the Shack-Hartmann wavefront sensor and Smirnov psychophysical method.

Subject	Age	Refractive error	Corrected visual acuity
LT	49	-0.25 -1.00 x 090	20 / 15
DH	29	-4.25 sphere	20 / 15

6.3

RESULTS

6.3.1 Shack-Hartmann sensor calibration

Prior to measuring human eyes, we tested accuracy of the S-H sensor with calibrated spherical wavefronts formed by introducing collimated light into lens L4 of the sensor branch, then focusing it to known distances by either moving lens L5 or by placing a lens over L5. The two test wavefronts had focal points located 3535 and 470 mm distal to the lenslets. A 5.6-mm-diameter beam was analyzed. The measured wavefronts were fitted to Zernike polynomials, and the wavefront elevation contributed by the 4th mode, representing defocus, was isolated. The 4th Zernike mode contains a constant term, which was factored out to make the wavefront height in the pupil center equal to zero. The resulting wavefronts, which represented measured defocus, were compared with the expected wavefront based on the known focal

distances. Errors, defined as measured minus expected wavefront heights, were calculated at approximately 150 points within the pupil. Table 6.2 summarizes parameters of the two calibrated wavefronts and the accuracy results. RMS wavefront measurement errors were $\sim\lambda/33$ and $\sim\lambda/50$. Corresponding dioptric equivalents were -0.008 and 0.006 D. This level of accuracy was at least as good as the accuracy with which we could measure either the lens power or focal distances used to create the test wavefronts. It was well below the maximum instrument error (0.17 D) reported by Liang and Williams (1997) and indicated that my apparatus itself was highly accurate.

TABLE 6.2 Parameters describing spherical test wavefronts used for calibration of the Shack-Hartmann wavefront sensor and measurement errors. Beam diameters were 5.6 mm.

Test wavefront radii (mm)	Wavefront edge height (λ)	Number of points sampled	Measured wavefront radii (mm)	RMS wavefront error (λ)	Error in diopters
3535	2.0	147	3636	.03	-0.008
470	13.8	148	469	.02	0.006

6.3.2 Human eye wavefronts measured by the Shack-Hartmann apparatus

Figure 6.4 shows raw images, mean wavefront aberration, and standard error contour plots for subject LT (left-hand column) and DH (right-hand column). Figs. 6.4a, and 6.4d are examples of typical raw images. Centrally the dots were bright and round, but peripherally some dots were dim and distorted. This variance in dot contrast and shape was more pronounced in LT. To speed up the centroid finding algorithm, images were filtered to brighten the dimmer dots before proceeding. The resulting dots were more uniformly bright, but scattered artifacts appeared near the pupil edges. The mean wavefronts were interpolated to draw smooth wavefront aberration contour plots (Figs. 6.4b, and 6.4e). In Fig. 6.4b, aberrations are larger, and contour lines indicate $1\text{-}\lambda$ intervals. Here subject LT's astigmatism is apparent by the vertically elongated contour lines that are most clearly evident in the temporal (figure left) half pupil. The nasal half pupil contained additional irregular aberrations that were subsequently investigated more thoroughly as will be described in Section 6.3.4. The wavefront aberration values are smaller in Fig. 6.4e, which shows $0.3\text{-}\lambda$ intervals. The more nearly circular contours are consistent with the lack of astigmatic refractive error for subject DH, although some asymmetry in the contours is evident. The lower plots, which show standard errors, use contour intervals of 0.25λ and 0.10λ (Figs. 6.4e, and 6.4f). Mean

standard errors for these plots were $\sim\lambda/2$ and $\sim\lambda/5$ for LT and DH, respectively. Comparing the standard errors and raw images, we see that between-measurement variance in the aberration function was greatest in the peripheral parts of the pupil where the wavefront slopes were greatest and dots were dimmest.

6.3.3 Comparison of wavefront aberration profiles measured psychophysically and with the Shack-Hartmann wavefront sensor

Figure 6.5 directly compares one-dimensional wavefront profiles measured by the two methods. Prism and spherical components were mathematically removed to reduce variance due to fluctuations in accommodation or small eye movements, and, indeed, I found a better match between the two curves after these were removed. S-H mean wave aberrations ($n=5$) are shown by the filled circles, and the squares indicate the mean Smirnov wavefront profiles for LT ($n=2$) and DH ($n=5$). For both subjects, the wavefront profiles measured by the two methods agreed closely in terms of shape, and centrally the curves were nearly superimposed. Except for the nasal (Fig. 6.5, right) half of LT's pupil and two points near the nasal edge of DH's pupil, the difference between the curves was less than $\sim\lambda/4$. RMS differences were $\sim\lambda/2$ for LT and $\sim\lambda/6$ for DH. Error bars indicate one standard error for the S-H measurements, and, except for the extreme nasal part of LT's pupil, most standard errors were smaller than $\lambda/4$. The mean standard errors were $\sim\lambda/7$ and $\sim\lambda/22$ for LT and DH respectively. The magnitude and shape of these wave aberrations are consistent with those reported elsewhere (Charman, 1991; Liang, *et al.*, 1994; Liang & Williams, 1997). The wavefront profiles in Fig. 6.5 show a central zone that is free of significant aberrations surrounded by increasing aberrations that reach a maximum of $2-4 \lambda$ at the pupil edge. If we adopt Rayleigh's quarter-wavelength rule for a well-corrected optical system (Born & Wolf, 1980), the critical pupil diameter within which diffraction rather than aberrations limit optical quality is approximately 3.0 mm for my subjects. In comparison, the median critical diameter for 55 subjects in Howland's subjective aberroscope study (Howland & Howland, 1977) was 2.8 mm, and for 11 subjects measured using an objective aberroscope the mean was 3.3 mm (Walsh, *et al.*, 1984).

The relative contribution of each primary and secondary aberration to the one-dimensional S-H wavefront aberrations are summarized in Table 6.3. Mean values for the coefficients B_2, B_3, B_4, B_5 (corresponding to primary coma, primary spherical, secondary coma and secondary spherical aberration, respectively) may be used to compute the wavefront slopes in radians by Eq. (6-1) and to compute the wavefront aberrations in micrometers using Eq. (6-2). For these coefficients, the pupil dimensions represented by variable u in Eq. (6-1) and (6-2), must be expressed in micrometers. For each component aberration, wavefront variance and longitudinal ray aberration in diopters for a marginal ray (5.6 mm pupil) are also listed in Table 6.3, and they show the relative contribution of each of aberration. Primary spherical

was the dominant aberration, more so in subject DH than in subject LT, and the dioptric expressions of longitudinal spherical aberration (bold type) agree with the range of values reported in other studies (Thibos, Ye, Zhang, & Bradley, 1997).

TABLE 6.3 Mean coefficients used in Eqs. (6-1) and (6-2) and other parameters describing 5th order polynomial fits to Shack-Hartmann wavefront slope data. Coefficients are associated with primary coma (B_2), primary spherical aberration (B_3), secondary coma (B_4), and secondary spherical aberration (B_5). Longitudinal aberration is computed for a 5.6 mm pupil marginal ray. Bold type highlights primary spherical aberration.

Coefficient	Mean (n=5)	Wavefront variance (λ^2)	Longitudinal aberration (diopters)
Subject LT			
B_2	5.895×10^{-11}	.08	.17
B_3	7.932×10^{-14}	.36	0.62
B_4	-1.359×10^{-17}	.07	-0.30
B_5	2.801×10^{-21}	.01	0.17
Subject DH			
B_2	-1.395×10^{-11}	0.00	-0.04
B_3	1.289×10^{-13}	0.94	1.01
B_4	2.180×10^{-18}	0.00	0.05
B_5	-6.402×10^{-21}	0.06	-0.39

The components aberrations are plotted in Fig. 6.6. For subject LT, primary spherical aberration alone (filled circles) closely approximates the total wavefront aberration (solid curve). Considered separately, both primary and secondary coma are sizeable aberrations relative to primary spherical, but in combination they contribute little to the overall aberration function since they have nearly equal magnitudes but opposite sign. Had data been limited to only first order aberrations, the resulting wavefront would have erroneously appeared to be more asymmetrical. In contrast to measurements by other methods, aberroscope measurements (Howland & Howland, 1977; Walsh, *et al.*, 1984) have generally found large comatic aberrations in the wave aberration functions, which could be exaggerated in some cases by the fact that second-order coma and higher aberrations are generally not measured by the aberroscope. The example of subject LT's wavefront profile demonstrates that methods to measure the wavefront aberration should be

capable of measuring aberrations beyond the first order, and this requires an instrument with a sufficiently fine sampling rate. This is a relative advantage of the S-H sensor, which can sample the pupil in intervals as small as 0.2 mm, and it can analyze aberrations up to at least the tenth order (Liang & Williams, 1997). A small amount of positive secondary spherical aberration was present in LT's eye. For DH, primary spherical is the dominant aberration, and the comas are negligible, though it is possible that coma could have been larger had some meridian other than the horizontal midline been measured. Beyond 2 mm from the pupil center, secondary spherical aberration for both subjects becomes significant, and, in the case of DH, its negative sign negates some of the primary spherical aberration.

6.3.4 Subtle local aberration detected by both methods

During the psychophysical experiment, subject LT observed that when the pinhole was translated horizontally in the nasal half of his pupil a fixed LED appeared subjectively to trace out a looplike trajectory indicative of a highly irregular aberration. Subsequently I searched for objective evidence of this refractive anomaly in the psychophysical data by tracking changes in the x and y wavefront slopes as the pinhole moved across the pupil. The abscissa of Fig. 6.7 represents wavefront slopes in the x direction, and the ordinate represents wavefront slopes in the y direction. Symbols indicate the slopes in these two orthogonal directions at each point along a horizontal traverse of the pupil, and numbers adjacent to selected symbols indicate sampled pupil locations. Thus the dashed line connecting the diamond shaped symbols represents a trajectory of slopes parameterized by pupil position as measured by the Smirnov technique. To obtain independent, objective evidence of this anomaly I reexamined the slope data from the S-H experiment, and the result is shown by the solid line in Fig. 6.7, which represents the corresponding trajectory as measured by the objective S-H method. Both results confirm the looping trajectory which the subject reported in the nasal side of his pupil. Additionally, the pupil locations at which miniscule and abrupt slope changes occur correspond relatively well between the two methods. A change in slopes of this kind in the x and y dimensions suggests an unusual aberration beginning near the pupil center and extending nasally along the midline. Reviewing the two-dimensional wavefront plot for subject LT (Fig. 6.4b), we see a confluence of irregular depressions in the wavefront aberration in the corresponding region, which is delineated in Fig. 6.4b by the rectangular overlay .

6.4

DISCUSSION

In theory the S-H wavefront sensor should provide highly accurate measurements of the aberrations of any optical system, including the human eye. We have verified this expectation for spherical calibration

wavefronts by showing that a S-H apparatus assembled from stock optical components is capable of measuring wavefront shape with RMS measurements errors of $\sim\lambda/30$ or less. Good repeatability for the wavefront profiles in an eye with relatively smoothly changing aberrations (Fig. 6.4e) was indicated by a mean standard deviation ($n = 5$) of $\sim\lambda/10$. This is similar to the $\sim\lambda/12$ mean standard deviation reported by Liang and Williams (Liang & Williams, 1997) for subject JL, who also had smoothly changing aberration contours. They used cycloplegic drops to paralyze accommodation, and three images, taken within 60 seconds, were averaged. In my experiments no cycloplegia was used, and the subject dismounted the bite bar for several minutes between S-H measurements. It was encouraging, therefore, to encounter similar low levels of variability despite the relaxed conditions of my experiments.

Lacking an absolute method for assessing accuracy of the S-H apparatus when used with human eyes, I estimated relative accuracy by directly comparing wave aberration profiles measured by the S-H method with those measured psychophysically by the Smirnov technique. The very close correspondence which I found (Fig. 6.5) is strong evidence that they are measuring the same thing: the wavefront aberration functions of the tested eyes. The RMS difference between the two methods was $\sim\lambda/5$ (Fig. 6.5, bottom) in the eye with smoother wave aberration contours (Fig. 6.4e) and lower between-measurement variance (Fig. 6.4f). Where the wavefront aberration was larger, measurement variance was also larger, especially near the margins of the pupil. Some of this increased variance may have been due to poorer image quality in parts of the S-H images. Also, the extended time required to collect the psychophysical wavefront data made the subjective results more susceptible to temporal fluctuations (e.g., tear film changes or accommodation).

The largest difference between wavefront aberration functions measured by the two methods was found in the nasal (Fig. 6.4b, right) half of LT's pupil. For this subject, the temporal half of the wavefront aberration function appears to be dominated by regular astigmatism (Fig. 6.4b), and in this region the wavefront measured by the two techniques were almost perfectly superimposed, with an RMS difference of $\sim\lambda/9$ (Fig. 6.5, top). In the nasal half, however, the difference between wavefront aberrations was much larger with an RMS difference of $\sim 2\lambda/3$. The most likely explanation for this large difference was the presence of localized, irregular aberrations in the nasal half of the pupil. Because the aberration function changes dramatically just above and just below the horizontal midline of this subject's pupil, slight vertical discrepancies between the locations of the horizontal traverses in the two experiments could have introduced large differences in results. For this reason the detailed vertical and horizontal wavefront slope changes shown in Fig. 6.7 are more revealing. The looplike traces in Fig. 6.7 correspond with shallow depressions in the wavefront aberration function (Fig. 6.4b) that were less than $\lambda/2$ deep. The subtle optical anomalies were not measurable by clinical refraction or slit lamp biomicroscopy of the ocular media, yet it was conspicuous in the wavefront slopes measured by both methods. Interestingly, a similar aberration was

noted in the same pupil location for this subject several years earlier when he sat for a chromatic aberration experiment (Simonet & Campbell, 1990), which suggests that this subtle refractive anomaly is a permanent feature in this subject's eye.

In conclusion, these results indicate that the Shack-Hartmann wavefront sensor can provide accurate and repeatable measurements of the wavefront aberration function of human eyes and that these measurements are in good agreement with independent measurements determined by the traditional Smirnov psychophysical technique. The two methods appear to be equally sensitive for detecting subtle irregular aberrations of the eye. Considering its numerous advantages of speed, objectivity, and high spatial resolution, I believe the Shack-Hartmann wavefront sensor is an attractive, valid instrument for basic and applied studies of the optical quality of the human eye.

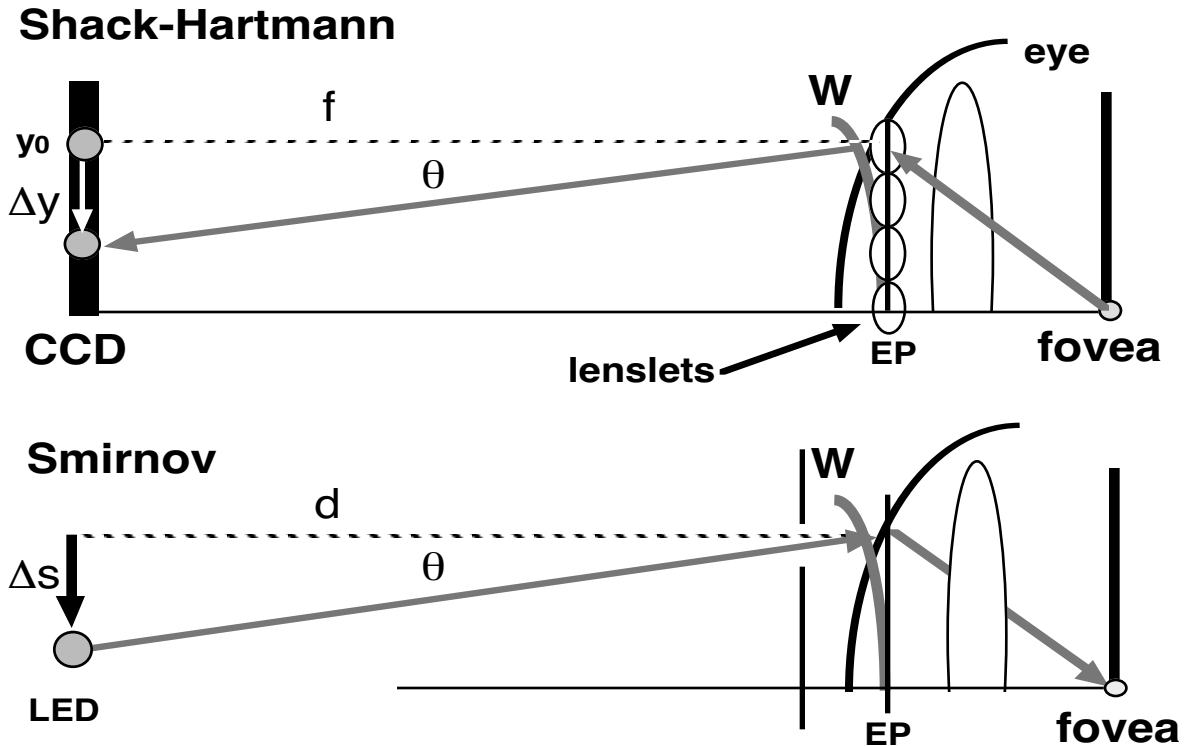


Figure. 6.1

Principle of wavefront sensing in the Shack-Hartmann (top) and Smirnov psychophysical (bottom) apparatus. (Δy = displacement of point image from reference position, f = focal length of lenslet. Δs = displacement of point object from the reference axis, and d = object distance) In the Shack-Hartmann (S-H) apparatus, a point source is placed on the fovea, and light is reflected out of the eye. The optical system relays an image of the eye's entrance pupil to the plane of an array of microlenslets that in effect, samples the emerging beam in the entrance pupil (EP). For the purposes of illustrating the principle the lenslet array is shown inside the eye in the plane of the entrance pupil, though the optical sampling of the entrance pupil actually occurs outside the eye. In a theoretical aberration-free eye, a bundle of rays is isolated by a lenslet and rays converge to point y_0 on the CCD. For an aberrated eye the image is displaced from reference point y_0 by an amount Δy and the ray deviation angle $\theta = \Delta y/f$. In the Smirnov method rays from a distant axial point object are isolated by a pinhole near the eye, and in the aberration-free case, these rays converge on the fovea. In the aberrated eye, the subject must displace the object by an amount Δs in order to center its image on the fovea. Here the ray deviation angle $\theta = \Delta s/d$. Both methods measure the same angle θ , which is the ray aberration at the isolated pupil location. Since rays are orthogonal to wavefronts, θ also represents the slope of the wavefront W in object space, from which W may be derived by integration.

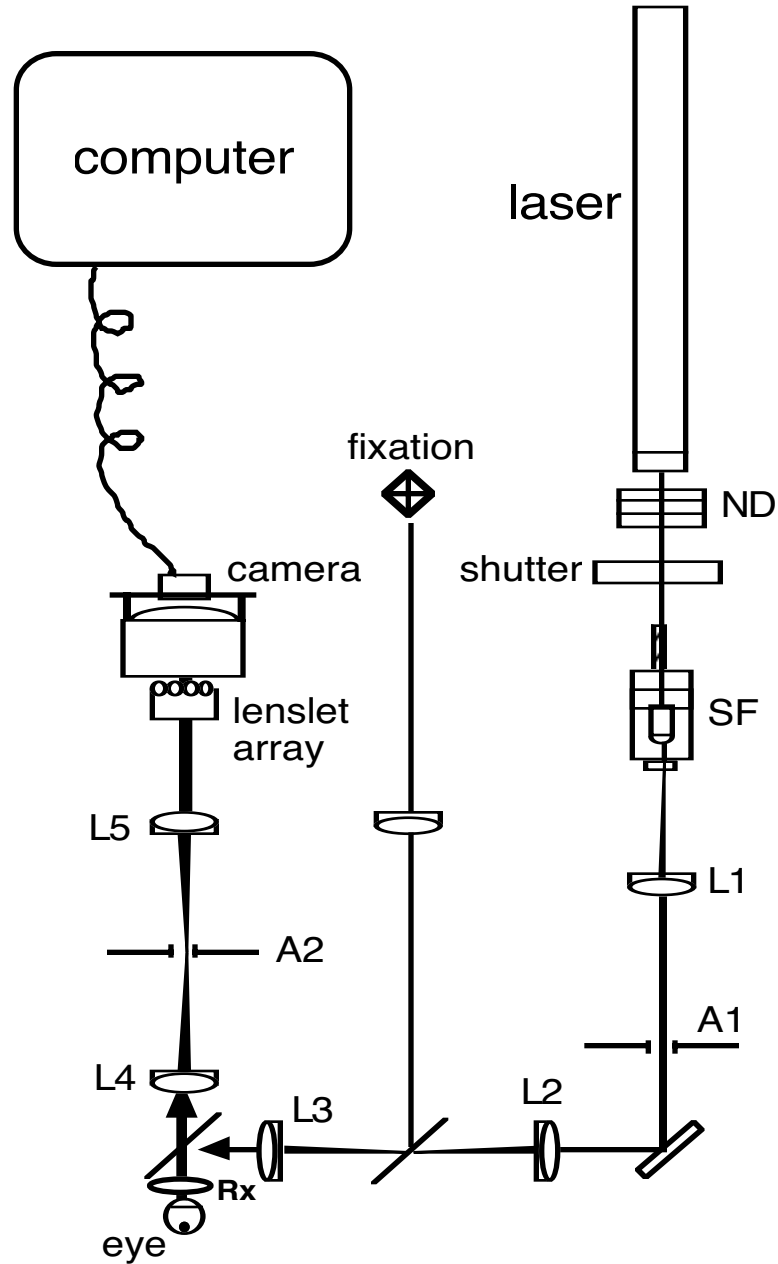


Figure 6.2

Shack-Hartmann wavefront sensor layout. A laser beam passes through neutral density filters (ND), an electronic shutter, spatial filter (SF), lenses L1-L3, lens Rx and the eye's optics to form a point of light on the fovea. The subject observes a fixation target during measurement. Light reflected off the retina passes out of the eye, through lenses Rx, L4 and L5 so that an image of the pupil is formed in the plane of the microlenslet array, and each lenslet forms an image of the retinal spot on the CCD. A confocal aperture, A2, prevents corneal reflections from reaching the camera while transmitting light from the retina. Digital images are stored on a computer, and are analyzed to reconstruct the eye's wavefront aberration function.

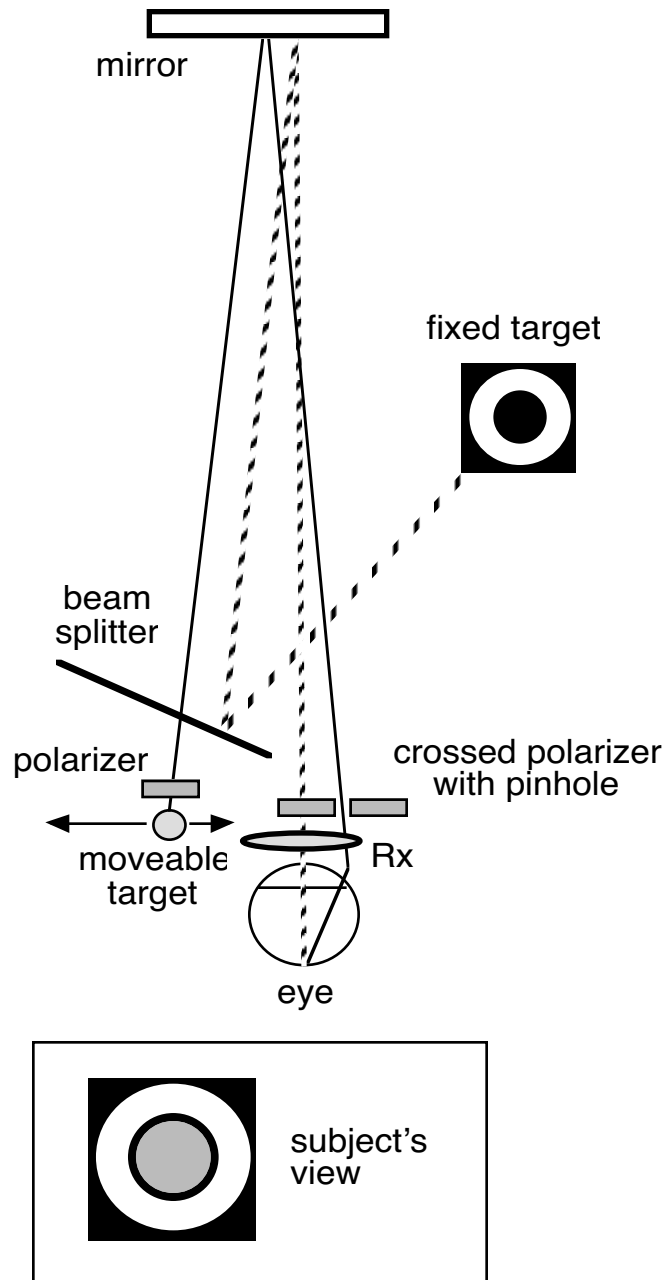


Figure 6.3

Psychophysical apparatus based Smirnov's principle. The subject observes a fixed annular target through his entire pupil while polarized light from an LED enters the pupil only through a small pinhole aperture drilled in a cross polarized filter that is positioned in front of the eye. The pinhole is used to isolate predetermined locations within the pupil, and for each position the subject adjusts the LED until it appears centered in the annulus, making it conjugate with the fovea. The positions of the LED and pinhole allow computation of the wavefront slope for the pupil location isolated by the pinhole, as described in Fig. 6.1.

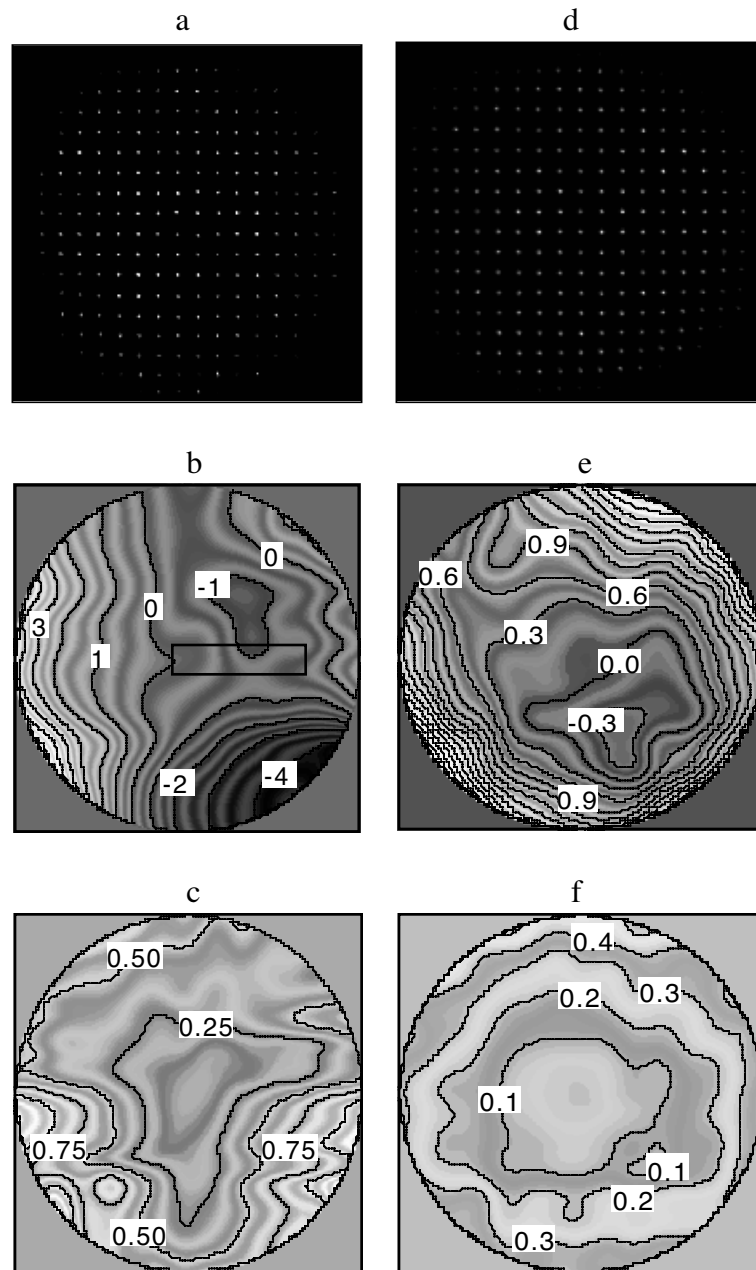


Figure 6.4

Two-dimensional wavefront aberration data from the Shack-Hartmann wavefront sensor. Data for subject LT is shown in the left column (a,b,c). The right column (d,e,f) shows data for DH. Example of raw data images are shown in the first row (a,d). The middle row shows mean ($n = 5$) wavefront aberration maps for LT (b) with 1λ contour intervals and for DH (e) with 0.3λ intervals. The rectangle in b delineates the region that contains a subtle wavefront anomaly described in detail in the text and graphed in Fig. 6.7. Corresponding standard error maps are shown for LT (c) with 0.25λ contour intervals and for DH (f) with 0.1λ intervals. Pupil diameters were 5.6 mm.

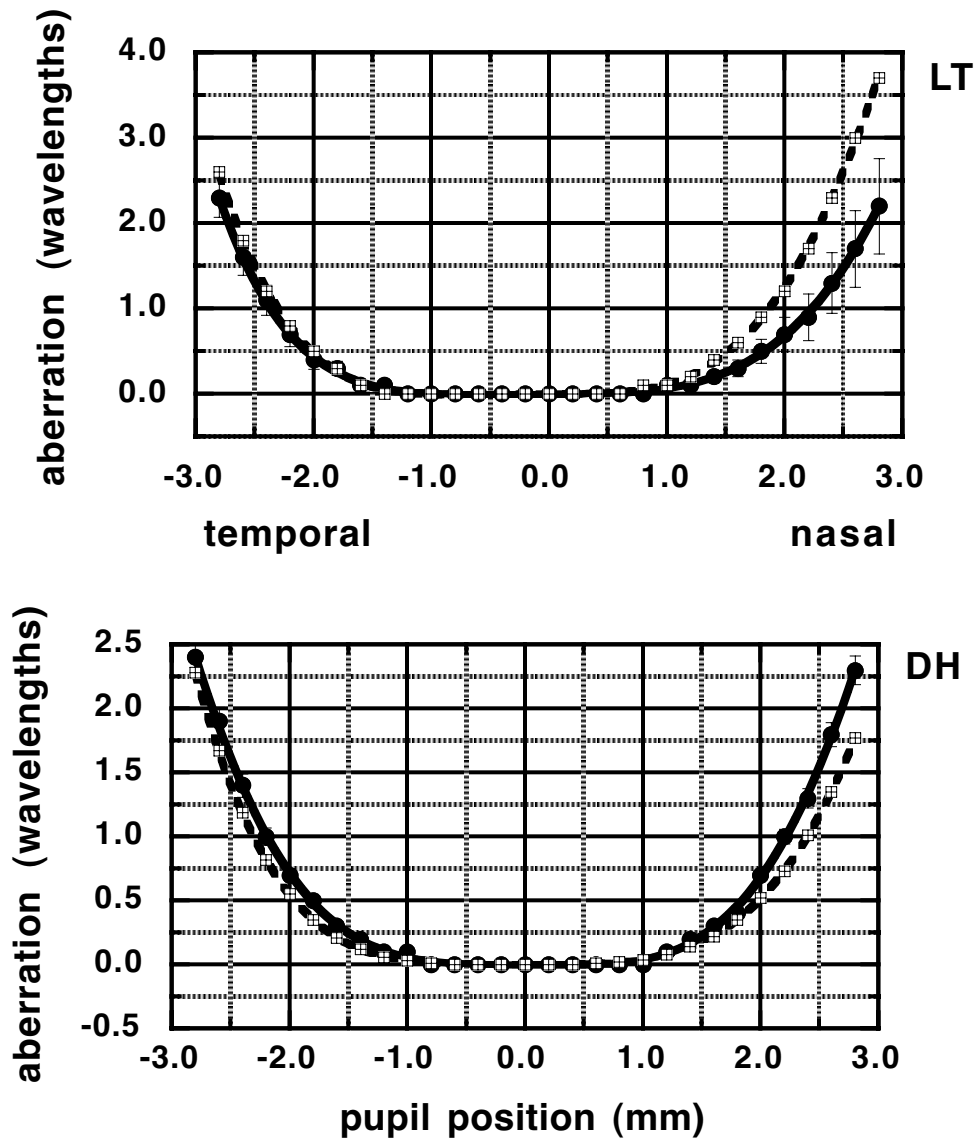


Figure 6.5

Direct comparison of wavefront aberration profiles measured by the Shack-Hartmann sensor (solid curve, circles) and Smirnov apparatus (dashed curve, squares) for subjects LT (top) and DH (bottom). Prism and defocus were removed, leaving only higher order aberrations for the comparison. The wavefront aberration in wavelengths ($\lambda = 632.8$ nm) across the 5.6 mm diameter pupils show close agreement between the two methods in terms of shape and magnitude. The greatest difference between the two techniques is noted in the nasal portion of LT's pupil.

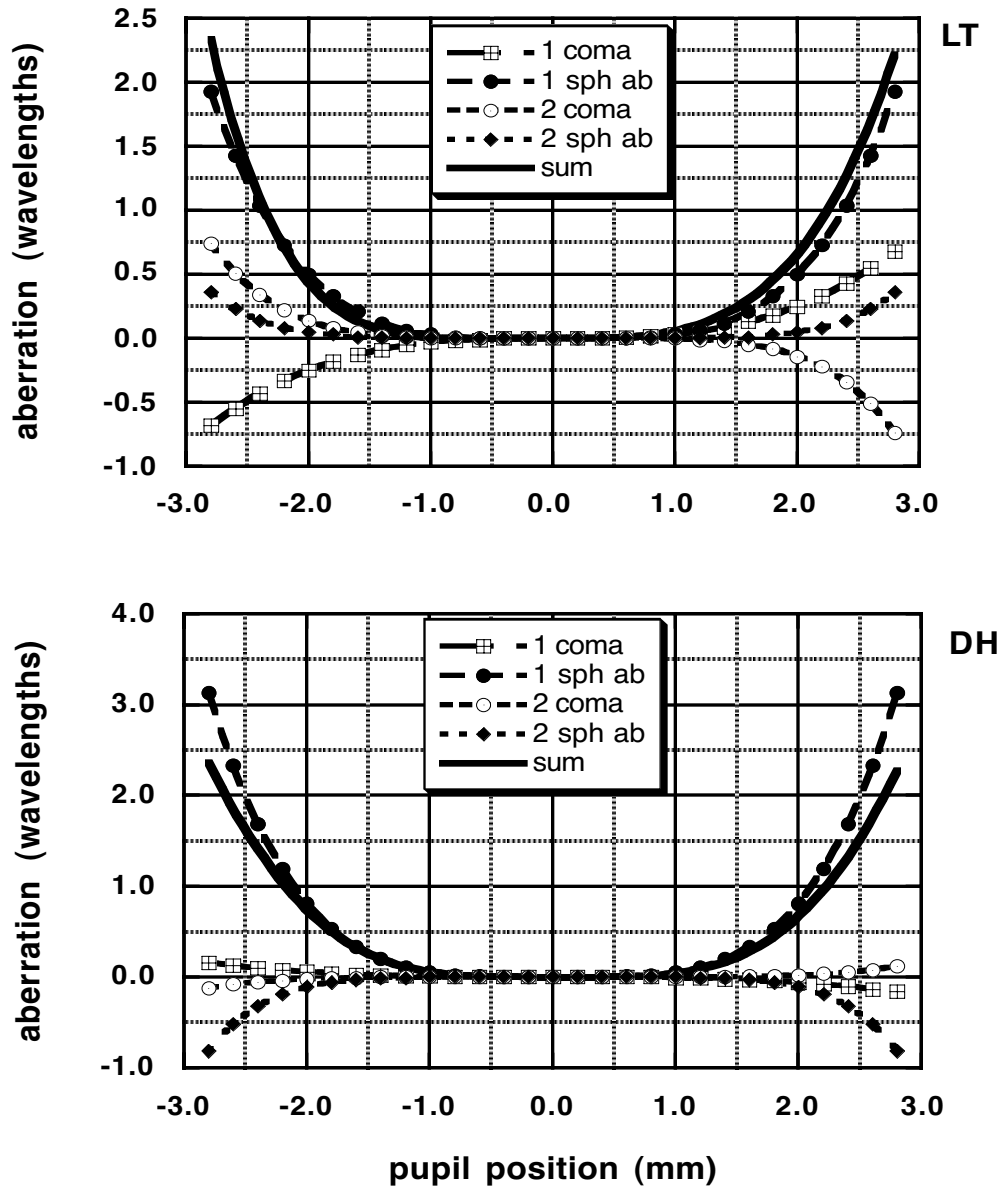


Figure 6.6

The relative contribution of primary coma (squares), primary spherical aberration (filled circles), secondary coma (open circles) and secondary spherical aberration (filled diamonds) to the total wavefront aberration profile (solid line) for subject LT (top) and DH (bottom). For LT, primary spherical aberration alone closely approximates the total aberration function. Combined primary and secondary coma make a minimal contribution to the total aberrations since they have similar magnitude but opposite signs and cancel each other out. A small amount of positive secondary spherical aberration is also present. For DH, primary spherical aberration also dominates, while primary and secondary coma are negligible. A small amount of negative secondary spherical aberration partially negates the large positive primary spherical aberration in the peripheral pupil.

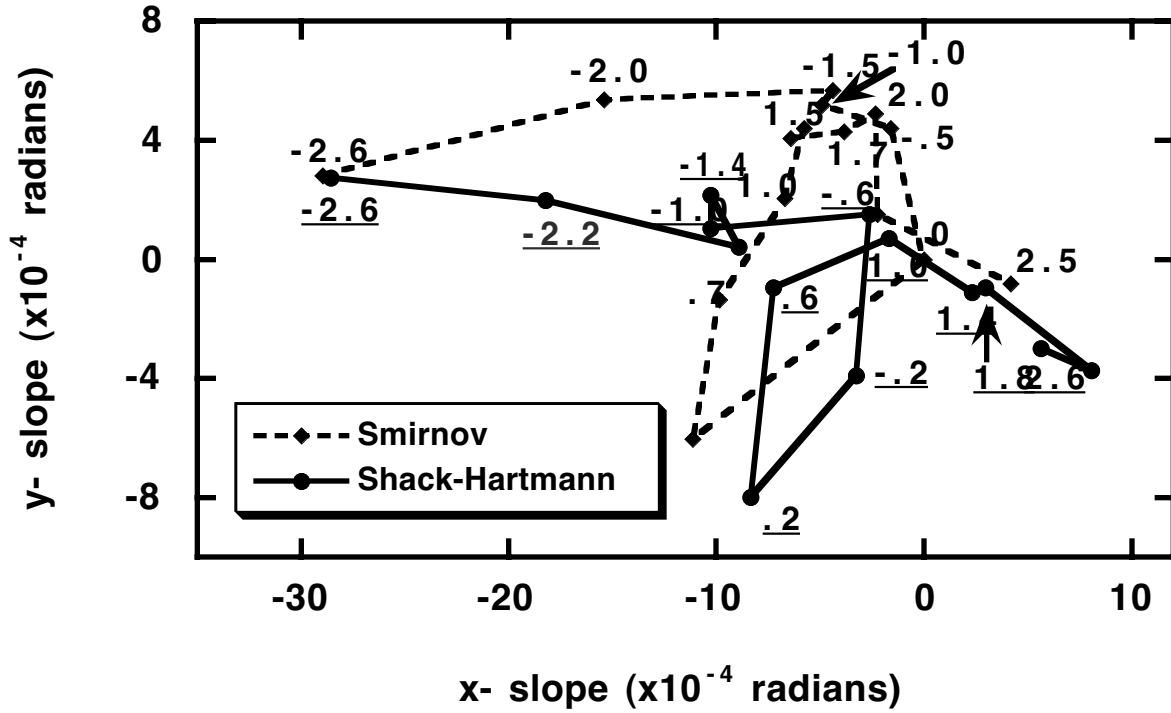


Figure 6.7

During psychophysical measurements of LT's wavefront aberration function, he observed that, as the pinhole moved horizontally across the nasal half of his pupil, a fixed LED appeared to move in a loop-like trajectory. This unusual aberration was verified in both the psychophysical (dashed line) and Shack-Hartmann (solid line) measurements and is visualized by plotting the x and y wavefront slopes measured at successive points across the pupil. Numbers near selected symbols indicate the horizontal distance in mm of each sample point from the pupil center. Negative values indicate the temporal half-pupil; positive, the nasal. Labels for the Shack-Hartmann data are underlined. Though slightly shifted from each other, both curves show the same loop-like reversal in the same part of the pupil where the pattern was noted subjectively. Additionally, miniscule and abrupt changes in wavefront slopes occur at corresponding pupil locations in both traces.